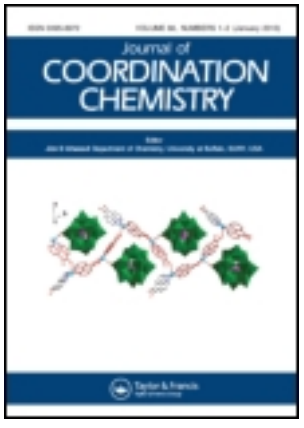

Journal of Coordination Chemistry
Publication details, including instructions for authors and subscription information:
http://www.tandfonline.com/loi/gcoo20

Four inorganic-organic hybrid complexes built from tetravanadate and macrocyclic oxamide

Yaqiu Sun [a], Yanyan Xu [a], Shangyuan Liu [a], Jing Wang [a], Dongzhao Gao [a] & Guoying Zhang [a]

[a] Tianjin Key Laboratory of Structure and Performance for Functional Molecules; Key Laboratory of Inorganic-Organic Hybrid Functional Material Chemistry, Ministry of Education; College of Chemistry, Tianjin Normal University, Tianjin, People's Republic of China

Accepted author version posted online: 22 May 2013.Published online: 25 Jun 2013.

To cite this article: Yaqiu Sun, Yanyan Xu, Shangyuan Liu, Jing Wang, Dongzhao Gao & Guoying Zhang (2013) Four inorganic-organic hybrid complexes built from tetravanadate and macrocyclic oxamide, Journal of Coordination Chemistry, 66:14, 2516-2528, DOI: 10.1080/00958972.2013.807922

To link to this article: http://dx.doi.org/10.1080/00958972.2013.807922

Journal of Coordination Chemistry, 2013
Vol. 66, No. 14, 2516–2528, http://dx.doi.org/10.1080/00958972.2013.807922

Four inorganic–organic hybrid complexes built from tetravanadate and macrocyclic oxamide

YAQIU SUN*, YANYAN XU, SHANGYUAN LIU, JING WANG, DONGZHAO GAO and GUOYING ZHANG

Tianjin Key Laboratory of Structure and Performance for Functional Molecules; Key Laboratory of Inorganic-Organic Hybrid Functional Material Chemistry, Ministry of Education; College of Chemistry, Tianjin Normal University, Tianjin, People's Republic of China

(*Received 31 January 2013; in final form 28 March 2013*)

Four inorganic–organic hybrid compounds, $[M_2(CuL)_4(V_4O_{12})]\cdot 2H_2O$ (M = Co (**1**), Mn (**2**)), $[Mn_2(NiL)_4(V_4O_{12})]\cdot 2H_2O$ (**3**), and $[Zn_2(CuL)_4(V_4O_{12})]\cdot 2CH_3OH\cdot 2H_2O$ (**4**) (M′L, H_2L = 2,3-dioxo-5,6,14,15-dibenzo-1,4,8,12-tetraazacyclo-pentadeca-7,13-dien), have been synthesized and characterized by elemental analysis, IR, UV, fluorescence spectra, and X-ray diffraction analysis. Single-crystal X-ray analysis reveal that both $[V_4O_{12}]^{4-}$ and M_2V_4 adapt a chair-like configuration in four structures. The cyclovanadate group $[V_4O_{12}]^{4-}$ is a tetradentate bridging ligand linking two $[M(M'L)_2]^{2+}$ fragments, producing centroantisymmetric heterometallic hexanuclear $[M_2M'_4]$ complexes. The variable-temperature magnetic susceptibility measurements (2–300 K) of **1** and **2** show weak antiferromagnetic interactions.

Keywords: Inorganic–organic hybrid compound; Heterometallic complex; Magnetism; Macrocyclic oxamide complex

1. Introduction

Polyoxometalates possess structural diversity and applications in photochemistry, clinical chemistry, magnetism, electric devices, catalysis, and materials science [1–3]. As important subclasses of POMs, polyoxovanadates exhibit various geometrical structures and have diverse applications in many fields. Polyoxovanadates have been used as inorganic building blocks for construction of inorganic–organic hybrid complexes, providing access to complex, multifunctional materials [4–9]. As a representative polyoxovanadate species, cyclic tetravanadate $[V_4O_{12}]^{4-}$ can be used as a multidentate ligand to link cationic complexes. Three coordination modes have been reported, with $[V_4O_{12}]^{4-}$ bidentate, tridentate, or tetradentate through coordination of oxido groups (scheme 1) [10–18]. Although some $[V_4O_{12}]^{4-}$ bridged inorganic–organic hybrid complexes have been synthesized, controlling in the construction remains a challenge in crystal engineering. Especially, tetravanadate-supported complexes containing two different metal ions have not been reported.

*Corresponding author. Email: hxxysyq@mail.tjnu.edu.cn

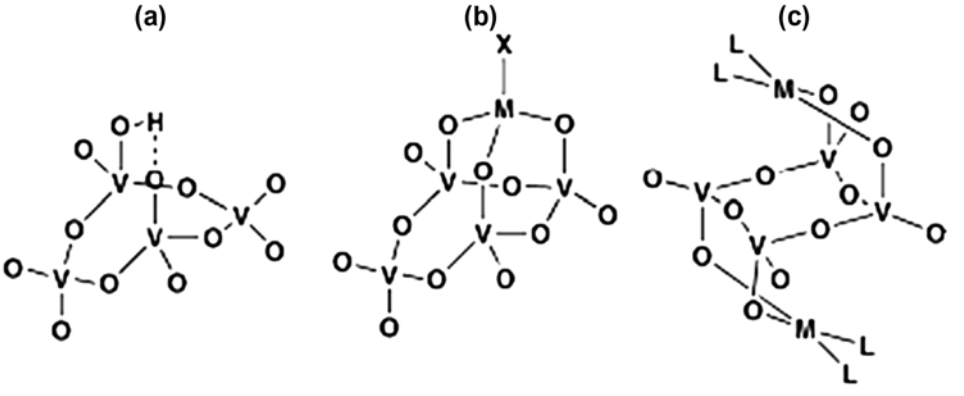

Scheme 1. The representative coordination modes of the cyclic tetravanadate.

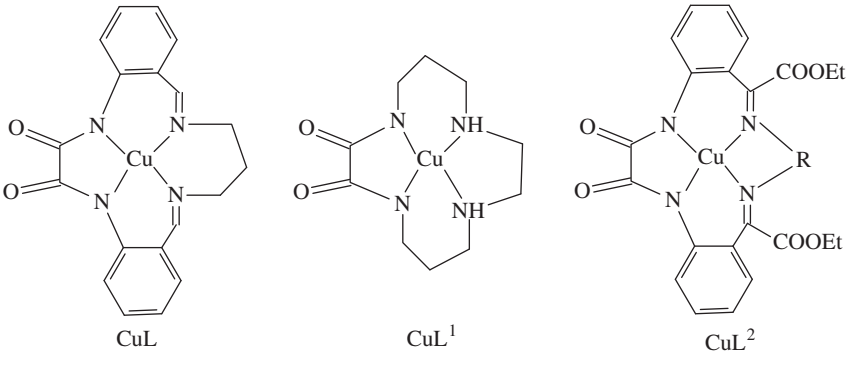

Scheme 2. The macrocyclic oxamide complex ligand.

Synthesis of homo- and heterometallic transition-metal complexes supported by oxamide bridges has attracted attention for architectural diversity and interesting properties. Noncyclic oxamides with various *N*,*N*′-substituents may adopt a *cis* or *trans* conformation on coordination, and this flexibility restricts control over the type of complex formed [19–23]. Macrocyclic oxamides, in which the exo-cis conformation of the oxygen donors is enforced, allow synthesis of homo- and heterobimetallic systems and model magnetic systems in a more controlled fashion via stepwise complexation of the macrocyclic and exo donors (scheme 2) [24–28]. To obtain heterometallic complexes, we have used macrocyclic oxamide complex and $[V_4O_{12}]^{4-}$ as co-ligand to coordinate with other metal ions. To the best of our knowledge, macrocyclic oxamides with polyoxovanadates as co-ligands have not been reported. Assembling complexes by polyoxovanadates and macrocyclic oxamides as co-ligands will open a new strategy to design inorganic–organic hybrid components. Herein, we report the syntheses, crystal structures, and magnetic properties of $[M_2(CuL)_4(V_4O_{12})]\cdot 2H_2O$ (M = Co (**1**), Mn (**2**)), $[Mn_2(NiL)_4(V_4O_{12})]\cdot 2H_2O$ (**3**), and $[Zn_2(CuL)_4(V_4O_{12})]\cdot 2CH_3OH\cdot 2H_2O$ (**4**).

2. Experimental

2.1. *Materials and physical measurements*

All starting reagents were of A. R. grade and used as purchased. The complex ligand ML (M = Cu, Ni) was prepared as described elsewhere [29]. Analyses of C, H, and N were determined on a Perkin-Elmer 240 Elemental Analyzer. IR spectra were recorded as KBr disks on a Shimadzu IR-408 infrared spectrophotometer from 4000 to 600 cm^{-1}. X-ray powder diffraction (XRPD) spectra were recorded on a Bruker D8 ADVANCE diffractometer with Cu K_α radiation ($\lambda = 0.15418$ nm). Electronic spectra for solid samples were recorded on a Shimadzu UV-2101 PC scanning spectrophotometer. Luminescence spectra for the samples were recorded with a Hitachi 850 fluorescence spectrophotometer. Variable-temperature magnetic susceptibilities of single crystals were measured on an MPMS-7 SQUID magnetometer. Diamagnetic corrections were made with Pascal's constants for all the constituent atoms [30].

2.2. *X-ray crystallography*

Single-crystal X-ray diffraction analyses of **1–4** were carried out on a Bruker Smart Apex II CCD diffractometer equipped with graphite-monochromated Mo-K_α radiation ($\lambda = 0.71073$ Å) by using ϕ/ω scan technique at room temperature. Semi-empirical absorption corrections were applied using SADABS. All structures were solved by direct methods using the SHELXS program of SHELXTL and refined with SHELXL. The crystallographic data and selected bond lengths and angles for **1–4** are listed in tables 1 and 2.

Table 1. Crystal data and structure refinement for **1–4**.

Complex	**1**	**2**	**3**	**4**
Formula	$C_{38}H_{36}CoCu_2N_8O_{12}V_2$	$C_{38}H_{36}Cu_2MnN_8O_{12}V_2$	$C_{38}H_{36}MnN_8Ni_2O_{12}V_2$	$C_{39}H_{38}Cu_2N_8O_{12}V_2Zn$
fw	1084.64	1080.65	1070.99	1105.10
Crystal system	Triclinic	Triclinic	Triclinic	Triclinic
Space group	*P*−*1*	*P*−*1*	*P*−*1*	*P*−*1*
a	10.495(4)	10.458(4)	10.545(3)	10.4832(12)
b	13.310(5)	13.471(5)	13.491(4)	13.2299(15)
c	16.215(6)	16.235(6)	16.279(5)	16.0445(18)
α, deg	95.007(6)	95.190(6)	94.843(6)	94.368(2)
β, deg	105.076(6)	104.873(6)	105.017(6)	105.025(2)
γ, deg	108.895(6)	109.047(6)	108.998(6)	108.822(2)
V, Å^3	2032.3(12)	2051.2(13)	2078.6(11)	2002.9(4)
Z	2	2	2	2
ρ_{calcd} g/cm^3	1.772	1.750	1.711	1.832
ν(Mo Kα) mm^{-1}	0.71073	0.71073	0.71073	0.71073
Crystal size (mm)	0.28 × 0.22 × 0.20	0.22 × 0.16 × 0.13	0.28 × 0.22 × 0.20	0.22 × 0.21 × 0.18
T, K	296(2)	296(2)	296(2)	296(2)
Goodness-F^2	1.042	1.086	1.031	1.054
$R1$[a] $[I > 2\sigma(I)]$	0.0381	0.0342	0.0624	0.0330
w$R2$[b] $[I > 2\sigma(I)]$	0.0884	0.1008	0.1373	0.0830

[a] $R1 = \sum ||F_o| - |F_c|| / \sum |F_o|$.

[b] $wR2 = \{\sum[w(F_o^2 - F_c^2)^2] / \sum[w(F_o)^2]\}^{1/2}$.

Table 2. Selected bond distances (Å) and angles (°) for **1–4**.

Compound **1**			
Co(1)–O(10)	2.030(3)	Co(1)–O(2)	2.172(3)
Cu(1)–N(4)	1.932(4)	Cu(1)–N(1)	1.934(4)
Cu(2)–N(8)	1.919(4)	Cu(2)–N(5)	1.958(4)
V(1)–O(6)	1.627(3)	V(1)–O(7)	1.795(3)
V(2)–O(8)	1.623(3)	V(2)–O(7)	1.811(3)
O(4)–Co(1)–O(3)	77.13(11)	O(4)–Co(1)–O(1)	177.97(12)
O(1)–Co(1)–O(3)	101.38(12)	O(4)–Co(1)–O(2)	105.26(12)
N(4)–Cu(1)–N(1)	94.02(16)	N(1)–Cu(1)–N(3)	159.88(18)
N(8)–Cu(2)–N(6)	166.23(16))	N(6)–Cu(2)–N(5)	86.34(14)
O(5)–V(1)–O(7)	110.33(15)	O(8)–V(2)–O(7)	110.50(16)
Compound **2**			
Cu(1)–N(1)	1.924(3)	Cu(1)–N(4)	1.929(3)
Cu(2)–N(8)	1.915(3)	Cu(2)–N(5)	1.955(3)
Mn(1)–O(5)	2.082(3)	Mn(1)–O(2)	2.261(3)
V(1)–O(6)	1.623(3)	V(1)–O(7)	1.792(3)
V(2)–O(8)	1.617(3)	V(2)–O(7)	1.803(3)
N(1)–Cu(1)–N(3)	159.64(15)	N(1)–Cu(1)–N(2)	87.02(13)
N(8)–Cu(2)–N(6)	166.89(13)	N(6)–Cu(2)–N(5)	86.37(12)
O(4)–Mn(1)–O(1)	175.89(10)	O(4)–Mn(1)–O(3)	73.76(9)
O(1)–Mn(1)–O(3)	102.17(10)	O(4)–Mn(1)–O(2)	107.51(10)
O(5)–V(1)–O(7)	110.53(13)	O(8)–V(2)–O(7)	110.97(14)
Compound **3**			
Mn(1)–O(5)	2.094(6)	Mn(1)–O(2)	2.265(6)
Ni(1)–N(3)	1.912(8)	Ni(1)–N(2)	1.936(8)
Ni(2)–N(7)	1.911(8)	Ni(2)–N(6)	1.965(7)
V(1)–O(6)	1.644(6)	V(1)–O(7)	1.789(6)
V(2)–O(8)	1.626(6)	V(2)–O(7)	1.827(6)
O(3)–Mn(1)–O(1)	176.0(2)	O(3)–Mn(1)–O(4)	74.4(2)
O(1)–Mn(1)–O(4)	101.7(2)	O(5)–Mn(1)–O(1)	83.1(2)
N(3)–Ni(1)–N(4)	92.5(4)	N(3)–Ni(1)–N(1)	159.8(4)
N(7)–Ni(2)–N(5)	166.5(3)	N(5)–Ni(2)–N(6)	86.4(3)
O(6)–V(1)–O(7)	111.0(3)	O(8)–V(2)–O(10)	108.7(3)
Compound **4**			
Cu(1)–N(3)	1.927(3)	Cu(1)–N(2)	1.964(3)
Cu(2)–N(5)	1.931(3)	Cu(2)–N(6)	1.938(3)
Zn(1)–O(5)	2.047(2)	Zn(1)–O(4)	2.184(2)
V(1)–O(6)	1.628(2)	V(1)–O(7)	1.801(2)
V(2)–O(9)	1.628(2)	V(2)–O(7)	1.812(2)
N(3)–Cu(1)–N(1)	166.00(12)	N(1)–Cu(1)–N(2)	86.25(11)
N(5)–Cu(2)–N(7)	159.92(12)	N(5)–Cu(2)–N(6)	87.00(11)
O(1)–Zn(1)–O(3)	176.42(9)	O(1)–Zn(1)–O(4)	105.59(9)
O(1)–Zn(1)–O(2)	77.63(9)	O(10)–Zn(1)–O(1)	94.15(9)
O(5)–V(1)–O(7)	110.24(11)	O(9)–V(2)–O(7)	110.84(11)

2.3. *Preparation of 1–4*

2.3.1. Synthesis of $[M_2(CuL)_4(V_4O_{12})]\cdot 2H_2O$ (M = Co (1), Mn (2)). A buffer layer of acetic ester was carefully layered over a distilled water (5 mL) solution of NH_4VO_3 (0.1 mM) and $M(CH_3COO)_2\cdot 4H_2O$ (0.1 mM). Afterward, a solution of CuL (0.1 mM) in methanol (5 mL) was layered over the buffer layer. The solution was left undisturbed at room temperature and after about five weeks brown crystals were obtained. Found: C, 42.06; H, 3.35; N, 10.33%. Calcd for $C_{38}H_{36}CoCu_2N_8O_{12}V_2$ **1**: C, 42.04; H, 3.32;

N, 10.32%. Found: C, 42.16; H, 3.34; N, 10.36%. Calcd for $C_{38}H_{36}Cu_2MnN_8O_{12}V_2$ **2**: C, 42.20; H, 3.33; N, 10.37%. Main IR bands (KBr, cm^{-1}): for **1**, 3403s (br), 1625s, 1561s, 1440 m, 1346 m, 1040 m, 927s, 820s, 710s; for **2**, 3436 m, 1650 m, 1607s, 1559s, 1476 m, 1081 m, 915s, 821s, 739(s).

2.3.2. Synthesis of $[Mn_2(NiL)_4(V_4O_{12})]\cdot 2H_2O$ (3). The reaction was carried out in a similar procedure as described for complex **2** except that NiL was used instead of CuL. After four weeks, deep red crystals were obtained. Found: C, 42.56; H, 3.35; N, 10.43%. Calcd for $C_{38}H_{36}MnN_8Ni_2O_{12}V_2$ **3**: C, 42.58; H, 3.36; N, 10.46%. Main IR bands (KBr, cm^{-1}): 3403s (br), 1628s, 1564s, 1474 m, 1343 m, 1037w, 923s, 825s 716s.

2.3.3. Synthesis of $[Zn_2(CuL)_4(V_4O_{12})]\cdot 2CH_3OH\cdot 2H_2O$ (4). The reaction was carried out in a similar procedure as described for **1** except that $Zn(CH_3COO)_2\cdot 4H_2O$ was used instead of $Co(CH_3COO)_2\cdot 4H_2O$. After five weeks, brown crystals were obtained. Main IR bands (KBr, cm^{-1}): 3441 m, 1636s, 1593s, 1478 m, 1339 m, 906s, 824s, 715s.

3. Results and discussion

3.1. *Synthetic and spectral aspects*

By using tetravanadate and macrocyclic oxamide mixed ligands as the metal linker, four new tetravanadate-supported heterometallic complexes have been synthesized. Generally, lowering the reaction speed may facilitate the slow growth of well-shaped larger single crystals suitable for X-ray diffraction. Considering this, the synthesis and isolation of **1–4** in this research were carried out through self-assembly of NH_4VO_3, $M(CH_3COO)_2\cdot 4H_2O$ (M = Co, Mn, Zn), and M′L (M′ = Cu, Ni) by using the slow diffusion method in a test tube under mild conditions of temperature and pressure. Complexes **1–4** are insoluble in water, methanol, carbon tetrachloride, chloroform, and benzene, but are appreciably soluble in acetone, DMF, and DMSO. In the solid state, **1–4** are all air stable. Elemental analyses of **1–4** are also consistent with the results of the structural analysis. All diffraction peaks of the experimental XRPD patterns of **1** and **2** (Supplemantary material) match well with the corresponding simulated ones obtained from single-crystal data, confirming their crystalline phase purity.

IR spectra of **1–4** were analyzed in a careful comparison with those of free mononuclear oxamide complex CuL or NiL. Complexes **1–4** are isostructural and have the same absorptions, hence only the IR spectra of **1** will be discussed as representative. The (C=O) and (C=N) stretching vibrations at 1642 and 1613 cm^{-1} for CuL are red shifted to 1627 and 1560 cm^{-1} for **1**, respectively, indicating that the oxygens of the carbonyl coordinate to another metal ion. The bands at 927 cm^{-1} are assigned to υ(V=O), and other strong peaks between at 820 and 710 cm^{-1} are attributed to υ(V–O–V) and υ(V–O–M), respectively [31] (Supplementary material).

The solid-state electronic absorption spectra of **1** and **2** were measured. The broad absorption at 523 nm can be assigned to the spin-allowed d–d electronic transition of Cu(II) ($3d^9$) in C_{4v} [32]. All complexes exhibit intense bands below 400 nm with the intense band at 260 nm of **1** and **2** attributed to intraligand π–π^* transition, while the moderately

intense band at 329 nm is assignable to charge-transfer transitions in the [CuL] chromophores [32].

Upon excitation at 340 nm, fluorescence spectra of **1** were measured in the solid state. Fluorescence spectra of **1** are given in Supplementary material. Complex **1** exhibits fluorescence at 486 nm. The band at 486 nm for **1** might be attributed to the LMCT (ligand-to-metal charge transfer) or MLCT (metal-to-ligand charge transfer) [33, 34].

3.2. *Structural description*

For **1–4**, $[M_2(M'L)_4(V_4O_{12})]$ are isostructural, where M = Co, M′ = Cu, **1**, M = Mn, M′ = Cu, **2**, M = Mn, M′ = Ni, **3**, M = Zn, M′ = Cu, **4**. The compounds present an M(II) center with a distorted octahedral geometry. It coordinates to four oxygens from two macrocyclic oxamides M′L and two oxygens from $V_4O_{12}^{4-}$. M′(II) resides in a slightly distorted square planar environment with two amidate nitrogens and two imino nitrogens from macrocyclic oxamide. The central M(II) is linked to each external M′(II) via the exo-cis oxygen donors of the macrocyclic oxamide. The three metal ions MM'_2 form a V-type arrangement through oxamide bridges with a Cu···Co average separation of 5.38 Å **1**, Cu···Mn average separation of 5.44 Å **2**, Ni···Mn average separation of 5.45 Å **3,** and Cu···Zn average separation of 5.35 Å **4**. The discrete $V_4O_{12}^{2-}$ cluster is constructed by four VO_4 tetrahedra connected through oxo (O_b) in such a way as to define an alternating V–O eight-membered ring, with one terminal oxygen (O_t) on each vanadium. The characteristic feature of these complexes is the planar conformation of the four vanadiums and the planar conformation of the four oxygens within the eight-membered ring. This endows the cluster with a twisted chair-like configuration. The cyclovanadate $[V_4O_{12}]^{4-}$ is a tetradentate bridging ligand to link two $[M(M'L)_2]^{2+}$ fragments, producing centroantisymmetric heterometallic hexanuclear $[M_2M'_4]$ complexes. M_2V_4 also forms a chair-like arrangement.

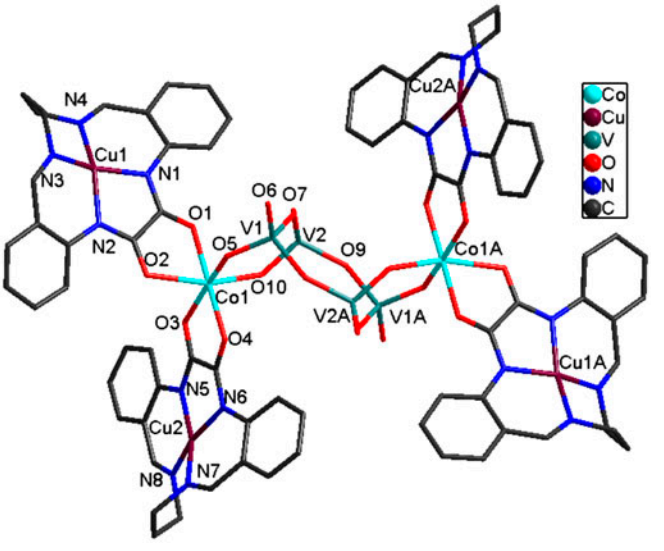

Figure 1. Perspective view of $[Co_2(CuL)_4(V_4O_{12})]$ unit (symmetry transformations used to generate equivalent atoms: A $1-x, 2-y, -z$).

A perspective view of the structure of $[Co_2(CuL)_4(V_4O_{12})]$ is depicted in figure 1, representating the isostructural group of **1–4**.

All V–O distances in **1–4** (1.623(3)–1.827(6) Å) are normal for $[V_4O_{12}]^{4-}$ and consistent with those reported previously. The V–O_t bond distances are short, ranging from 1.623(3) to 1.644(6) Å. The V–O_b bond lengths present short exocyclic V1–O5 distances (1.655(3) for **1**, 1.656(1) for **2**, 1.647(5) for **3,** and 1.663(2) Å for **4**) and short exocyclic V2–O10 distances (1.654(3) for **1**, 1.650(3) for **2**, 1.649(4) for **3,** and 1.650(2) Å for **4**), while the endocyclic V–O_b bond distances are 1.771(3)–1.827(6) Å.

All O–V–O bond angles are close to the tetrahedral angle, ranging from 105.98(1) to 111.19(2)°. All V–O–V angles within the ring have two values (121.78(2), 148.9(2) for **1**, 124.17(1), 149.83(2) for **2**, 123.6(3), 149.7(4) for **3**, and 121.12(1), 148.62(2) for **4**). Each compound has two different V–O–M angles (127.53(2), 136.72(2) for **1**, 128.27(14), 136.27(14) for **2**, 128.6(3), 137.2(3) for **3**, and 127.31(12), 136.81(13) for **4**) and the more obtuse angle associated with the short V–O_b distance.

Although the four complexes have the same coordination $[M_2(M'L)_4(V_4O_{12})]$, there are different intermolecular interactions. For **1** and **2**, the neutral $[M_2(M'L)_4(V_4O_{12})]$ units are bound together by O–H···O intermolecular hydrogen bonds to form a double one-dimensional chain (figure 2). The hydrogen bonding system in **1** and **2** consists of uncoordinated

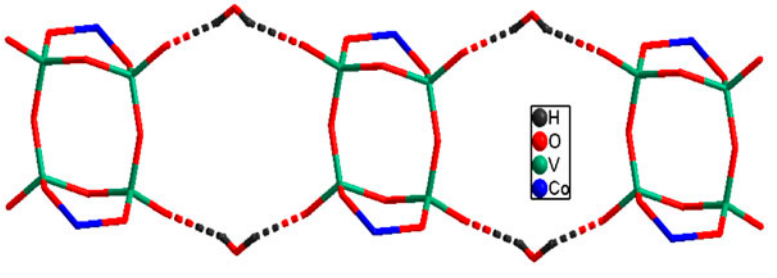

Figure 2. View of the one-dimensional chain motif formed by strong intermolecular hydrogen bonds in **1** (all hydrogens and a part of CuL were omitted for clarity).

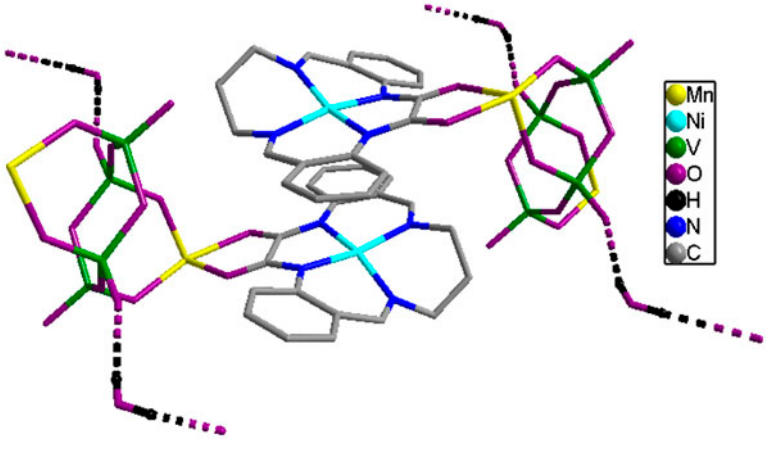

Figure 3. View of the self-assembly 1-D supramolecular architecture through O–H···O and weak π–π interactions for **3**.

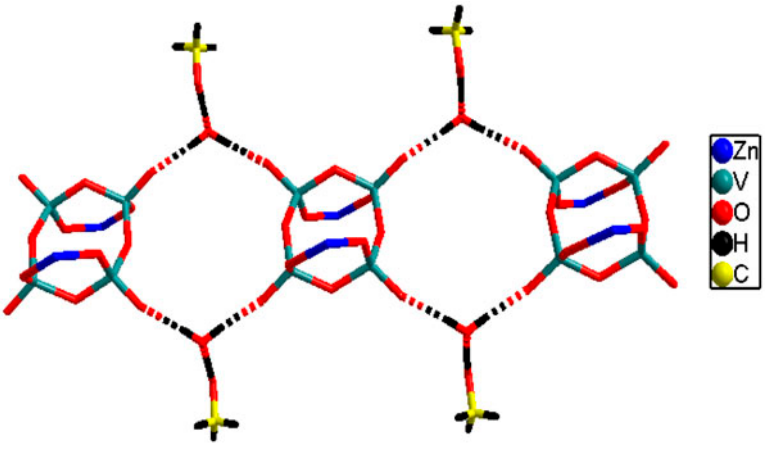

Figure 4. View of the one-dimensional chain motif formed by strong intermolecular hydrogen bonds in **4** (all hydrogens and a part of CuL were omitted for clarity).

Table 3. Hydrogen bond lengths (Å) and angles (°) for **1–4**.

	D–H···A	d(D–H)	d(H···A)	d(D···A)	DHA
Complex **1**	O(11)–H(11′)···O(8)[a]	0.852	2.057	2.881	162
	O(11)–H(11″)···O(6)[b]	0.850	2.489	2.844	106
Complex **2**	O(11)–H(11′)···O(8)[a]	0.850	2.024	2.849	163
	O(11)–H(11″)···O(6)[a]	0.852	2.110	2.825	141
Complex **3**	O(11)[a]–H(11′)···O(9)	0.859	2.086	2.896	157
Complex **4**	O(11)–H(11′)···O(9)[a]	0.850	1.993	2.842	176
	O(11)–H(11″)···O(6)[a]	0.850	1.951	2.800	176
	O(12)–H(12)···O(11)	0.820	1.764	2.578	171

Symmetry codes for **1**: (a) x, $y-1$, z; (b) $2-x$, $2-y$, $-z$; for **2**: (a) $x+1$, y, z; for **3**: (a) x, $-1+y$, z; for **4**: (a) $x+1$, $y+1$, z.

oxygens on $V_4O_{12}^{4-}$ combined with hydrogens on free water. The corresponding O···O distances are 2.844–2.881 Å for **1** and 2.826–2.848 Å for **2**, while the hydrogen bonding in **3** consists of hydrogens on the free water with oxygens on $V_4O_{12}^{4-}$. There are π–π interactions between benzene rings of NiL of different $[Mn_2(NiL)_4(V_4O_{12})]$ units in the cell, which are parallel to each other, and the distance between carbons is 3.416 Å (figure 3). For **4**, $[Zn_2(CuL)_4(V_4O_{12})]$ are alternately bridged by free water to form infinite chains through O–H···O interactions between $V_4O_{12}^{4-}$ and free free water ($d_{O\cdots O}=2.801$, 2.848 Å). In addition, there are other O–H···O interactions between free water and free methanol, with O···O distance of 2.577 Å (figure 4). Hydrogen bond lengths (Å) and angles (°) for **1–4** are listed in table 3.

3.3. *Magnetic properties*

The magnetization measurements for **1** and **2** have been carried out under 2 kOe. The $\chi_M T$ value of 3.80 $cm^3\,mol^{-1}\,K$ at 300 K for powder sample of **1** is larger than the spin-only value of 2.63 $cm^3\,mol^{-1}\,K$ expected for the uncoupled $Cu^{II}_2Co^{II}$ trinuclear system (figure 5). This indicates an important contribution from the orbital momentum typical for high-spin octahedral Co^{II} with a $^4T_{1g}$ ground state. By lowering the temperature, $\chi_M T$

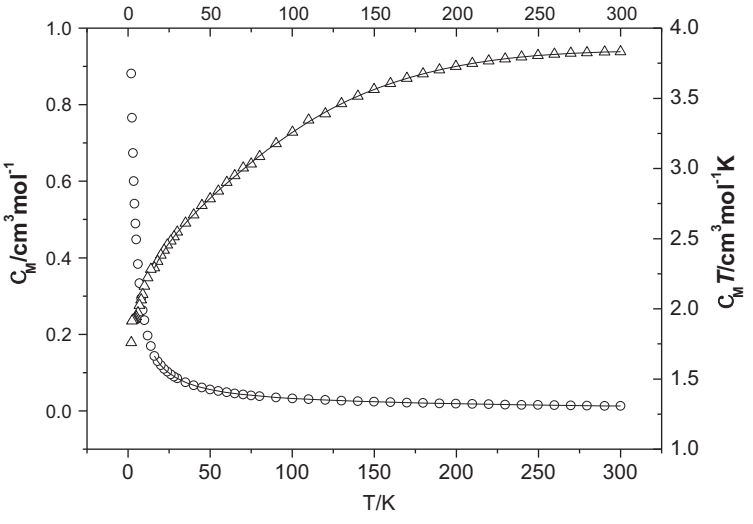

Figure 5. χ_M (O) *vs.* T and $\chi_M T$ (Δ) *vs.* T plots for **1**.

decreases continuously to $1.40\,cm^3\,mol^{-1}\,K$ at 2 K. The shape of the $\chi_M T$ *versus* T curve suggests overall antiferromagnetic behavior. On the basis of the crystal structure of **1**, in a first approach, the magnetic analysis was carried out by using the theoretical expression of the magnetic susceptibility deduced from the spin Hamiltonian $\hat{H} = -2J(\hat{S}_{Cu1}\hat{S}_{Co} + \hat{S}_{Cu2}\hat{S}_{Co})$.

$$\chi_{CoCu_2} = \frac{N\beta^2}{4KT}\left[\frac{35g_{5/2,1}^2 + 10g_{3/2,1}^2\exp(\frac{-5J}{KT}) + g_{1/2,1}^2\exp(\frac{-8J}{KT}) + 10g_{3/2,0}^2\exp(\frac{-3J}{KT})}{3 + 2\exp(\frac{-5J}{kT}) + \exp(\frac{-8J}{kT}) + 2\exp(\frac{-3J}{kT})}\right] \quad (1)$$

$$g_{\frac{5}{2},1} = (3g_{Co} + 2g_{Cu})/5 \quad g_{\frac{3}{2},1} = (11g_{Co} + 4g_{Cu})/15 \quad g_{\frac{1}{2},1} = (5g_{Co} + 2g_{Cu})/3 g_{\frac{3}{2},0} = (g_{Co})$$

where part of the orbital angular momentum of Co(II) is reflected in the temperature dependence of the g_{Co} factor equation (2) [35].

$$g_{Co} = \sqrt{\frac{3kT\chi_{Co}}{N\beta^2 S(S+1)}} \quad (2)$$

$$\chi_{Co} = \frac{N\beta^2}{3kT}\frac{F_1}{F_2}$$

$$F_1 = \frac{7\lambda(3-A)^2}{5kT} + \frac{12(2+A)^2}{25A} + \left[\frac{2\lambda(11-2A)^2}{45kT} + \frac{176(A+2)^2}{675A}\right]\exp\left(\frac{-5A\lambda}{2kT}\right) + \left[\frac{\lambda(A+5)^2}{9kT} - \frac{20(A+2)^2}{27A}\right]\exp\left(\frac{-4A\lambda}{kT}\right)$$

$$F_2 = \frac{\lambda}{3kT}\left[3 + 2\exp\left(\frac{-5A\lambda}{2kT}\right) + \exp\left(\frac{-4A\lambda}{kT}\right)\right]$$

Then, magnetic interactions between adjacent trinuclear Cu_2Co units bridged by $V_4O_{12}^{4-}$ are evaluated using molecular field approximation equation (3).

$$\chi_M = \chi_{CoCu_2}/[1 - \chi_{CoCu_2}(2zj'/Ng^2\beta^2)] \quad (3)$$

In equations (1–3), J is the exchange integral between Cu(II) and Co(II) through oxamido bridge and zJ' stands for the intermolecular exchange integral between Cu_2Co trinuclear units. A is ligand field parameter ($A=1$, strong field limit; $A=1.5$, weak field limit) and λ is spin-orbit coupling parameter ($\lambda=-170\,cm^{-1}$ for free cobalt(II)). The least-squares fit to the experimental data lead to best parameters of $J=-0.79\,cm^{-1}$, $g_{Cu}=2.0$ (fixed), $zJ'=9.44\times10^{-3}\,cm^{-1}$, $A=1.31$, and $\lambda=-170\,cm^{-1}$ (fixed), the agreement factor defined as $R=\sum[(\chi_M)^{Cal}-(\chi_M)^{obsd}]^2/\sum[(\chi_M)^{obsd}]^2$ is 1.017×10^{-6}. The point below 15 K cannot be reproduced with this model, possibly due to the limitation of the model of the complex. The fitted results show that spin-orbit coupling of Co(II) plays an important role in magnetic behavior.

$\chi_M T$ of $5.2\,cm^3\,mol^{-1}\,K$ at 300 K for powder sample **2** is close to the spin-only value of $5.26\,cm^3\,mol^{-1}\,K$ expected for a four spin system of $S=1/2$, $S=5/2$, $S=1/2$, indicating that all the metal ions are high-spin (figure 6). By lowering the temperature, $\chi_M T$ decreases continuously and reaches $1.75\,cm^3\,mol^{-1}\,K$ at 2 K. Based on the crystal structure of **2** (figure 1), the coupling topology should be considered as Cu_2Mn trinuclear units. Then, the molecular field approximation was used for magnetic interactions between adjacent trinuclear units. The magnetic susceptibility expression for the trinuclear unit Cu_2Mn can be derived from the spin Hamiltonian: $\hat{H}=-2J(\hat{S}_{Cu}\hat{S}_{Mn}+\hat{S}_{Cu}\hat{S}_{Mn})$, where J is the exchange integral between Cu(II) and Mn(II) through the oxamido bridge. The expression of the magnetic susceptibility was obtained as follows:

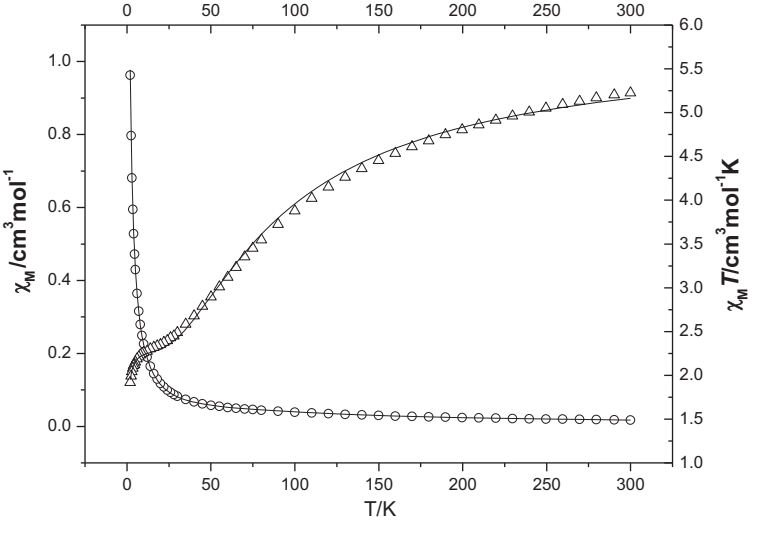

Figure 6. χ_M (O) *vs.* T and $\chi_M T$ (Δ) *vs.* T plots for **2**.

$$\chi_{tri} = \frac{N\beta^2}{4kT}\frac{A}{B}$$

$$A = 10g_1^2 + 35g_2^2\exp\left(\frac{5J}{kT}\right) + 35g_{\mathrm{Mn}}^2\exp\left(\frac{7J}{kT}\right) + 84g_3^2\exp\left(\frac{12J}{kT}\right)$$

$$B = 2 + 3\exp\left(\frac{5J}{kT}\right) + 3\exp\left(\frac{7J}{kT}\right) + 4\exp\left(\frac{12J}{kT}\right)$$

$$g_1 = (7g_{\mathrm{Mn}} - 2g_{\mathrm{Cu}})/5$$

$$g_2 = (31g_{\mathrm{Mn}} + 4g_{\mathrm{Cu}})/35$$

$$g_3 = (5g_{\mathrm{Mn}} + 2g_{\mathrm{Cu}})/7$$

The magnetic interactions between adjacent trinuclear Cu_2Mn units bridged by $V_4O_{12}^{4-}$ are evaluated using the molecular field approximation equation (3).

$$\chi_M = \chi_{tri}/[1 - \chi_{tri}(2zj'/Ng^2\beta^2)] \quad (4)$$

The least-squares fit to the experimental data was found with $J = -14.8\,\mathrm{cm}^{-1}$, $zj' = -0.10\,\mathrm{cm}^{-1}$, $g_{\mathrm{Cu}} = 2.0$ (fixed), and the agreement factor defined as $R = \sum[(\chi_M)^{Cal} - (\chi_M)^{obsd}]^2/\sum[(\chi_M)^{obsd}]^2$ is 1.23×10^{-5}.

For **1** and **2**, antiferromagnetic interaction through oxamido arises from nonzero overlap between the magnetic orbital around Cu(II) and Co(II) (**1**) or Mn(II) (**2**). The oxamido bridge promotes a very weak antiferromagnetic interaction between Cu(II) and Co(II) ions, compared with some cobalt(II)-copper(II) species incorporated by macrocyclic oxamide ligands reported previously; the exchange integral in **1** is smaller than those reported [27, 36, 37]. The weak antiferromagnetic coupling observed for **1** can be rationalized by the geometry parameters. The difference between the magnetic exchange may be explained on the basis of structural distortions and distances. One relevant factor is the value of the dihedral angle (γ) between the mean equatorial plane of the metal ion and the oxamido plane [38, 39]: the greater the value of γ the smaller the antiferromagnetic coupling. Complex **1** has a larger value of γ(14.8) and longer distance of Cu···Co (5.38 Å), which benefit a weak antiferromagnetic coupling. Larger steric hindrance of $V_4O_{12}^{4-}$ and oxamide groups destroy the planar structure of the two magnetic orbitals of Cu(II) and Co(II), which led to reduction in the overlap integral between the magnetic orbitals, and resulted in a relatively small antiferromagnetic coupling constant. The obtained zj' values make it possible to conclude that the antiferromagnetic coupling is very weakly transmitted through the vanadate bridge, due to the large M–M distances in **1** and **2**.

4. Conclusions

Using vanadate co-ligands as the starting material, based on slow diffusion method, four oxamido-bridged macrocyclic complexes were synthesized. The present work provides a new exploration on the design and construction of diverse heteropolynuclear inorganic–organic hybrid complexes. Complexes **1** and **2** show weak antiferromagnetic exchange interactions between the adjacent metal centers.

Supplementary material

Crystallographic Data (excluding structure factors) for the structures reported in this paper have been deposited with the Cambridge Crystallographic Data Center as supplementary publication numbers CCDC 904910-904913.

Acknowledgements

This work was supported by the National Natural Science Foundation of China (Nos. 20771083, 20901059, 21001081 and 21043004) and Tianjin Normal University (No. 52XC1102).

References

[1] Polyoxometalate Chemistry: *From Topology via Self-Assembly to Applications*, M.T. Pope, A. Müller (Eds), Kluwer: Dordrecht, The Netherlands (2001).
[2] D.L. Long, E. Burkholder, L. Cronin. *Chem. Soc. Rev.*, **36**, 105 (2007).
[3] W.G. Klemperer, T.A. Marquart, O.M. Yagi. *Angew. Chem. Int. Ed.*, **31**, 49 (1992).
[4] H.Y. Ma, X. Meng, J.Q. Sha, H.J. Pang, L.Z. Wu. *Solid State Sci.*, **13**, 850 (2011).
[5] Y. Hayashi. *Coord. Chem. Rev.*, **255**, 2270 (2011).
[6] M.A. Sedgwick, D.C. Crans, N.E. Levinger. *Langmuir*, **25**, 5496 (2009).
[7] M. Aureliano. *Dalton Trans.*, **42**, 9093 (2009).
[8] W. Ouellette, G. Wang, H. Liu, G.T. Yee, C.J. O'Connor, J. Zubieta. *Inorg. Chem.*, **48**, 953 (2009).
[9] M.I. Khan, R.C. Nome, S. Deb, J.H. McNeely, B. Cage, R.J. Doedens. *Cryst. Growth Des.*, **9**, 2848 (2009).
[10] V. Paredes-García, S. Gaune, M. Saldías, M.T. Garland, R. Baggio, A. Vega, M. Salah El Fallah, A. Escuer, E. Le Fur, D. Venegas-Yazigi, E. Spodine. *Inorg. Chim. Acta*, **361**, 3681 (2008).
[11] D. Attanasio, F. Bachechi, L. Suber. *J. Chem. Soc., Dalton Trans.*, 2373 (1993).
[12] T. Kurata, Y. Hayashi, K. Isobe. *Chem. Lett.*, **38**, 218 (2009).
[13] V.W. Day, W.G. Klemperer, A. Yagasaki. *Chem. Lett.*, **19**, 1267 (1990).
[14] H. Akashi, K. Isobe, Y. Ozawa, A. Yagasaki. *J. Cluster Sci.*, **2**, 291 (1991).
[15] M. Abe, K. Isobe, K. Kida, A. Nagasawa, A. Yagasaki. *J. Cluster Sci.*, **7**, 103 (1996).
[16] M. Abe, K. Isobe, K. Kida, A. Nagasawa, A. Yagasaki. *J. Cluster Sci.*, **5**, 565 (1994).
[17] M. Abe, K. Isobe, K. Kida, A. Yagasaki. *Inorg. Chem.*, **35**, 5114 (1996).
[18] Y. Hayashi, N. Miyakoshi, T. Shinguchi, A. Uehara. *Chem. Lett.*, **29**, 170 (2000).
[19] H.H. Lu, Y.T. Li, Z.Y. Wu, K. Zheng, C.W. Yan. *J. Coord. Chem.*, **64**, 1360 (2011).
[20] S.H. Cui, M. Jiang, Y.T. Li, Z.Y. Wu, X.W. Li. *J. Coord. Chem.*, **64**, 4209 (2011).
[21] L.H. Xu, H.X. Wang, L.N. Zhu. *J. Coord. Chem.*, **65**, 1051 (2012).
[22] Y.J. Zheng, X.W. Li, Y.T. Li, Z.Y. Wu, C.W. Yan. *J. Coord. Chem.*, **65**, 3530 (2012).
[23] B.L. Liu, J. Dang, G.P. Li, R.J. Tao. *J. Coord. Chem.*, **64**, 1931 (2011).
[24] L. Cronin, A.R. Mount, S. Parsons, N. Robertson. *J. Chem. Soc., Dalton Trans*., 1925 (1999).
[25] S.B. Wang, G.M. Yang, D.Z. Liao, L.C. Li. *Inorg. Chem.*, **43**, 852 (2004).
[26] L.N. Zhu, N. Xu, W. Zhang, D.Z. Liao, K. Yoshimura, K. Mibu, Z.H. Jiang, S.P. Yan, P. Cheng. *Inorg. Chem.*, **46**, 1297 (2007).
[27] Y.Q. Sun, D.Z. Gao, W. Dong, D.Z. Liao, C.X. Zhang. *Eur. J. Inorg. Chem.*, **2825**, (2009).

[28] Y.Q. Sun, L.L. Fan, D.Z. Gao, Q.L. Wang, M. Du, D.Z. Liao, C.X. Zhang. *J. Chem. Soc., Dalton Trans.*, 9654 (2010).
[29] D.S.C. Black, H. Corrie. *Inorg. Nucl. Chem. Lett.*, **12**, 65 (1976).
[30] P.W. Selwood. *Magnetochemistry.* p. 78, Interscience, New York, NY (1956).
[31] K. Nakamoto, *Infrared and Raman Spectra of Inorganic and Coordination Compounds*, 5th Edn., John Wiley, New York (1997), Part B.
[32] F. Lloret, Y. Journaux, M. Julve. *Inorg. Chem.*, **29**, 3967 (1990).
[33] X. Shi, G.S. Zhu, X.H. Wang, G.H. Li, Q.R. Fang, G. Wu, G. Tian, M. Xue, X.J. Zhao, R.W. Wang, S.L. Qiu. *Cryst. Growth Des.*, **1**, 207 (2005).
[34] X. Shi, G.S. Zhu, Q.R. Fang, G. Wu, G. Tian, R.W. Wang, D.L. Zhang, M. Xue, S.L. Qiu. *Eur. J. Inorg. Chem.*, **185**, (2004).
[35] H. Akashi, N. Uryǔ, T. Shibahara. *Inorg. Chim. Acta*, **53**, 261 (1997).
[36] Y.Q. Sun, D.Z. Gao, Y. Ma, G.M. Yang, D.Z. Liao, S.P. Yan. *J. Mol. Struct.*, **963**, 240 (2010).
[37] Y.Q. Sun, Y.Y. Xu, D.Z. Gao, G.Y. Zhang, Y.X. Liu, J. Wang, D.Z. Liao. *J. Chem. Soc., Dalton Trans.*, 5704 (2010).
[38] S. Alvarez, M. Julve, M. Verdaguer. *Inorg. Chem.*, **29**, 4500 (1990).
[39] J.L. Sanz, B. Cervera, R. Ruiz, C. Bois, J. Faus, F. Lloret, M. Julve. *J. Chem. Soc., Dalton Trans*., 1359 (1996).